International Forum on Aeroelasticity and Structural Dynamics
IFASD 2024
17-21 June 2024, The Hague, The Netherlands

GROUND VIBRATION TESTING AND MODEL UPDATE OF A TRANSONIC FLUTTER WIND TUNNEL MODEL

Anders Ellmo[1]

[1]Saab AB
Bröderna Ugglas Väg, Linköping, Sweden
anders.ellmo@saabgroup.com

Keywords: structural dynamics, aeroelasticity, model update

Abstract: Using complex composite structures in a wind tunnel model means that small differences in layup, thickness and other manufacturing outcomes will result in significant consequences for the structural dynamic properties of the model, and subsequently its aeroelastic behaviour. The KTH-NASA wind tunnel model has interchangeable wings composite wings, and it is shown that finite element representations of each individual wing are needed to match experimental data, and produce accurate predictions of flutter behaviour, [1].

1 INTRODUCTION

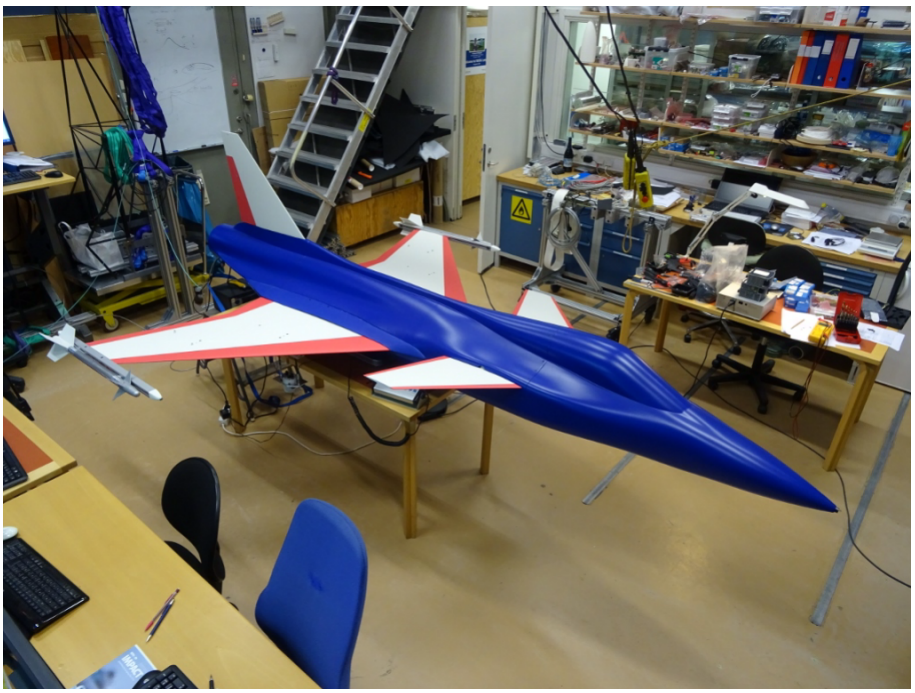

Figure 1: Overview of the KTH aeroelastic wind tunnel model.

A wind tunnel model for obtaining experimental data from aeroelastic testing at transonic conditions has been designed specifically for the NASA LaRC Transonic Dynamics Tunnel (TDT), see Figure 1. The model is equipped with pressure transducers, accelerometers and an extensive data acquisition system. It is a representation of a light weight single engine fighter with canards and delta wings. During 2016 it was subjected to aeroelastic testing in air and heavy gas in TDT and two flutter points were recorded before flutter of the wing tips damaged the

wing shell. While the wings were too damaged to allow further testing, the design was verified to be safe for testing since no material separated from the wing and there was no damage to the tunnel. [1]

The original wing was designed conservatively and found to flutter only with all external stores mounted. Therefore, a new wing structural design was created to allow for flutter inside the tunnel operating envelope without external stores under the wing. A design optimization process subject to aeroelastic stability constraints, and the desire to avoid introducing topological changes, resulted in a composite design for the wing shells that allows for flutter conditions within the TDT operating boundaries with just the wing tip missiles mounted. [2]

Three sets of wings were manufactured according to the updated design. The wings were built using CNC-milled moulds based on the CAD geometry. The wing skin layup was done by hand using a aluminium frame as an aid to obtain the correct angle of the unidirectional weave. A detailed description of the design and manufacturing process process is presented in [2].

This paper describes the modal testing of two wing pairs mounted on a full or partial aircraft structure (reference tests), and tap tests of each wing manufactured according to the new design. It also includes a subsequent model update procedure of each wing towards the test results from the tap tests. The updated finite element models are assembled with finite element representations of the entire aircraft structure and the full models dynamic properties is compared to the reference tests.

Finally, the flutter characteristics of the update finite element model are compared to those of the nominal model. In addition, we measure the spread of flutter dynamic pressure as a result of manufacturing uncertainties. This is an experimental approach to determining the probability distribution of the wings dynamic properties. An analytical approach with a similar intent has been performed by Stanford and Massey that treated a number of variables as random, and showed the impact on both elastic and inertial structural properties of the wing and also on flutter failure. [3]

2 TEST OBJECT DESCRIPTION

The wing consists of a composite sandwich with an internal fiberglass skeleton. The wing shells are a fibreglass epoxy laminate in five layers, with three layers made up of thin 80gr/m^2 Interglas 90070 plain weave and interspersed layers of thicker 200gr/m^2 Interglas 92145 unidirectional weave in the following layup: [0# 110- 135# 110- 0#]. The weave layup angles are mirrored across the mid-plane of the wing and the x-z-plane of the fuselage. Angle θ in Figure 2 is the angle of the unidirectional weave on the left side top shell. Inside the composite shell is a high density foam that is linear elastic to large strains and has a high failure strain, which creates a robust wing structure that keeps together in a flutter failure incident of limited amplitudes. The mid-plane of the wing has a skeleton made out of fibreglass laminate, the main purpose of which is to support concentrated loads from external stores mounted to the model. The layout of the fibreglass skeleton is illustrated in light gray in Figure 2.

As can be seen in Figure 2, pylons made from extruded aluminium profiles are attached to the wing tips. They are clamped to the fibreglass skeleton at two points. In the reference tests, a wing tip missile is attached to each pylon with bolts. The missiles contain a movable point mass that can be placed in either a forward or a rearward position to alter the structural dynamic properties of the aircraft. The altered dynamic properties is hopefully be enough to increase

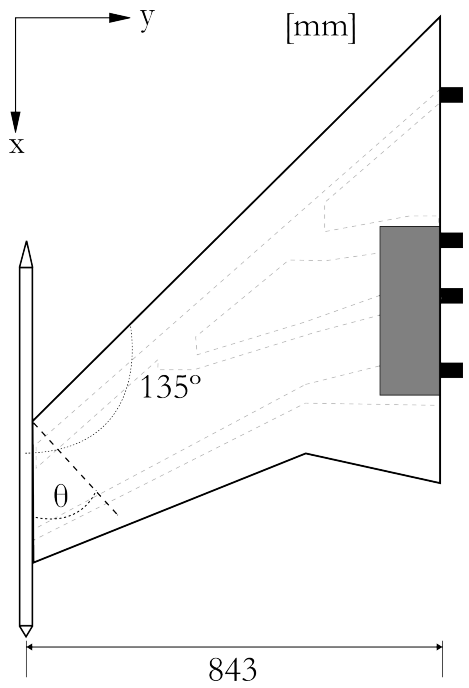

Figure 2: Structural layout of the left wing.

structural damping, should a critical flutter incident be encountered. The movable masses are placed in the forward position for both reference tests.

The wings are connected to the fuselage via three main bulkheads milled from aluminium, and a z-moment lug connected a forward bulkhead.

All bulkheads are attached to standard extruded aluminium profiles which together form the main fuselage and platform for the data acquisition and control systems. Tubes for pneumatic control of the movable of the wing tip missiles are fed through the wing assemblies to the systems located in the fuselage. The wing skins are drilled with rows of pressure taps, and stainless steel tubes are run from the fibreglass shell, through the foam down and along the mid-plane in order to have the smallest possible influence on wing stiffness. The tubes connect to the Optimus/Initium pressure scanner system in the fuselage, [4].

3 METHOD

3.1 Modal analysis

Curve fitting is done on the accelerance frequency response functions using the proprietary PolyMax algorithm, an implementation of the poly-reference Least-Squares Complex Frequency-domain (pLSCF) algorithm. [5] Frequency response functions are synthesized from experimental modes in order to assess the quality of the curve fit, and to track accelerometers with noisy data. Accelerometers with noisy data are deselected whenever they generate noise in the stabilization diagrams. The experimental modes are then exported to a universal file format for further processing.

The chosen set of modes is phase-corrected to remove mode complexity, and re-scaled to obtain generalized mass for each mode. Experimental modes are then matched with the analytical modes on frequency and mode shape. The Modal Assurance Criteria (MAC) is used to estimate the degree of correlation between an experimental and analytical mode shape. [6]

3.2 Optimization

The model update is focused on the results from the individual impact hammer tests and is expressed as the optimization problem

$$\begin{aligned} \min_{x_i} \quad & \sum_{i=1}^{n} (x_i - x_{0i})^2 \\ \text{subject to} \quad & f_j \leq f_j(\mathbf{x}) \leq \overline{f_j}, \qquad \forall j \in \xi, \\ & \underline{MAC_k} \leq MAC_k(\mathbf{x}), \qquad \forall k \in \kappa \\ & \underline{x_i} \leq x_i \leq \overline{x_i}, \qquad i = 1, \ldots, n \end{aligned} \tag{1}$$

where x_i and x_{0i} are the i:th design variable and the i:th nominal value, and $\underline{x_i}$, $\overline{x_i}$ are the bounds for the design variables. A set $\xi \in \mathbf{R}^m$, where m is the number of constrained eigenfrequencies, contains the constrained eigenfrequencies. The j:th eigenfrequency is denoted $f_j(\mathbf{x})$ and has a lower bound f_j and an upper bound $\overline{f_j}$. The k:th MAC constraint is denoted MAC_k and has a lower bound $\underline{MAC_k}$. The measured and calculated mode shapes that forms the constraints belongs to the set $\kappa \in \mathbf{R}^p$ where p denotes the number of MAC values. The formulation used is standard procedure in the Saab structural dynamics department [7].

4 EXPERIMENTAL MODAL TESTING

Two tests have been carried out with the wings mounted on either the full aircraft model mounted on the TDT sting or a partial aircraft model in a free-flying state suspended with elastic cord. These tests will be referred to as *reference tests*, as they will be used to evaluate the result of the model update. There is a third set of wings (2.2) that has been tested but since the wing pair is in a semi-finished state the results are not included here.

Additionally, each wing has been analyzed separately in free-free conditions and impact hammer excitation.

Some abbreviations are used to describe the mode shapes in Tables 2 and 3. These are described in Table 1 below.

Table 1: Abbreviations used for mode shape descriptions

Abbreviation	Full name
S	Symmetric
AS	Anti Symmetric
B	Bending
T	Torsion
W	Wing

4.1 Testing the first wing pair (2.0) - reference test A

The first experimental modal testing was carried out in the TDT test section. The full aircraft model with complete instrumentation was mounted on the tunnel sting, see Figures 3a and 3b. This test made use of the first new wing pair (2.0).

All fairings except the wing fairings were mounted, internal systems and ballasts were in the intended positions and the pneumatic system for moving external store masses was active, i.e.

in the state in which aeroelastic testing will be performed. The sting was held in place with the tunnels mechanical lock used during aeroelastic testing. The test object was excited by electro-dynamic shakers connected to the test object via adjustable push-pull rods, with force-transducers for measuring the input signal mounted with hot-glue on aluminium tape between the structure and the push-pull rods, see Figure 3c. The test was performed with a mobile LMS SCADAS Recorder 02 test system with 16 channels available. Siemens LMS Testlab 17 was used for data acquisition and control.

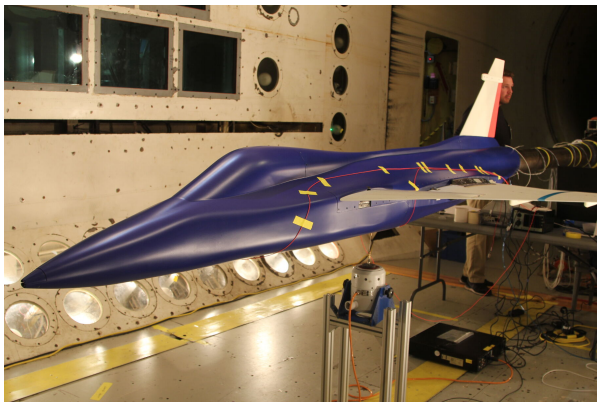

(a) The test object mounted on sting.

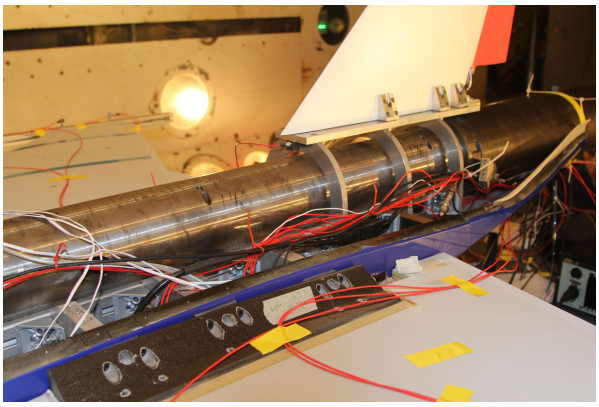

(b) Interface to the TDT sting.

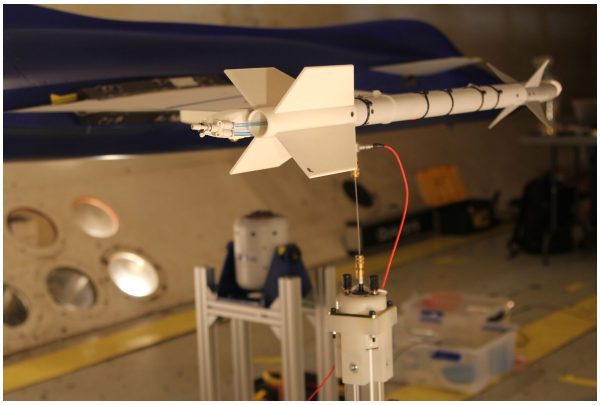

(c) Aft wing excitation point.

Figure 3: Photos from Reference test A.

Table 2: Results of Reference test A as compared to the nominal FE model

Experimental results			Nominal FE-model					
Mode #	Freq Hz	Gen mass kg	Mode #	Freq Hz	Gen mass kg	Freq diff %	MAC -	Description -
1	7.35	69	2	7.03	49	-4.3	0.8	System pitch *
2	9.66	3	3	10.21	1	5.7	0.99	ASWB
3	10.09	4	4	10.48	1	3.9	0.98	SWB
4	13.76	12	5	15.00	1	9.0	0.36	LWT (ASWT)
5	14.80	10	7	15.18	1	2.6	0.28	RWT (SWT)
8	46.45	7	15	56.11	3	20.8	0.86	2nd ASWB
9	52.22	2	16	61.60	2	18.0	0.81	2nd SWB

* Rigid pitching motion of both sting and model, caused by the sting mount.

The wing torsion modes, mode 4 and 5, appear as separate left and right wing torsion modes in the test, see Table 2. This is an indication that the left and right wing might have asymmetrical properties. The MAC-index between the finite element model and the experimental results is very low for these modes as the finite element model has symmetrical wings with clear symmetrical and anti symmetrical wing torsion modes.

4.2 Testing the second wing pair (2.1) - reference test B

Due to the results of the first reference test, a test of the second wing pair was carried out at Saab in Linköping. The second subset of the aircraft model consisting of the second set of wings (2.1), wing tip pylons, wing tip missiles and a part of the fuselage. The exact extent is shown in the schematic overview in Figure 4.

The aircraft was also tested with all external stores mounted, see Figure 5a and 5b, but those configurations are not included here.

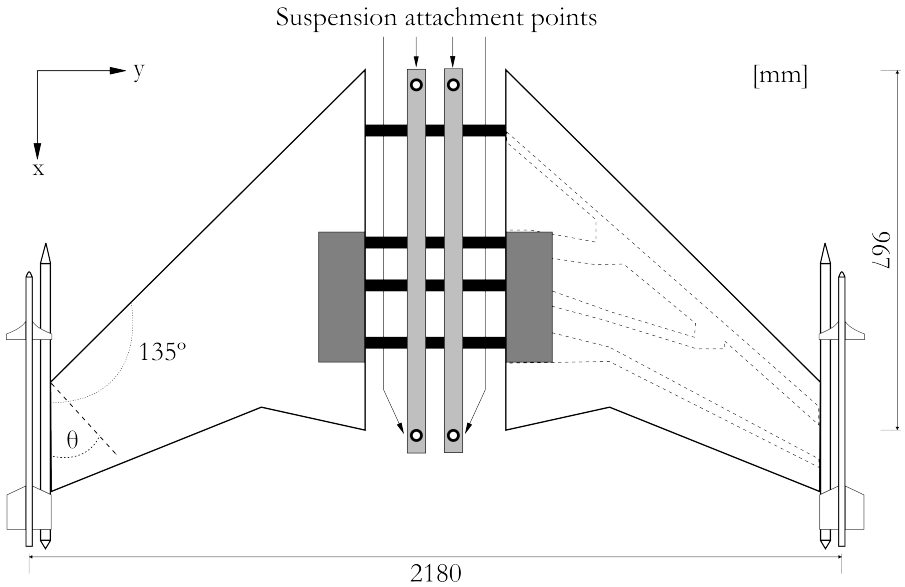

Figure 4: Structural layout of the test object.

The test object was suspended from the ceiling by elastic ropes connected to loops at the front and rear end of the structure, as shown in Figure 5a. The suspension was adjusted to create as much separation between the highest rigid body mode and the first elastic mode as possible. The deflection of the structure turned out to be larger than the maximum stroke length of the shakers for some modes, even at the lowest excitation level, which created artificial stiffness and a distorted response. Impact excitation was used as a complement for these modes, a method that does not introduce artificial stiffness to the structure.

The finite element model was modified to be a representation of the test object by changing or removing substructures that are partly or completely left out in this configuration, for example the fuselage shell, canards and the fin. During assembly of the test object each component and substructure was weighed separately, and the complete test object was weighed after assembly. The measured mass data was used to update the mass of the components in the finite element model accordingly. After the mass update the model updating process only considers the stiffness properties.

Accelerometers were mounted in locations chosen to have the highest total response for the

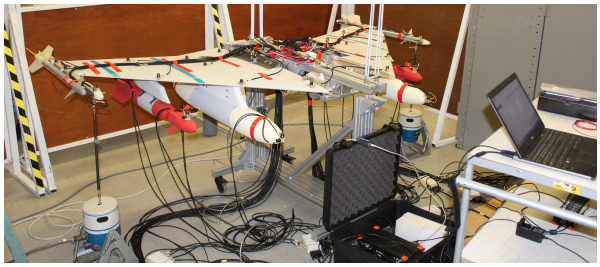

(a) The test object mounted at Saab, in a configuration with all external stores.

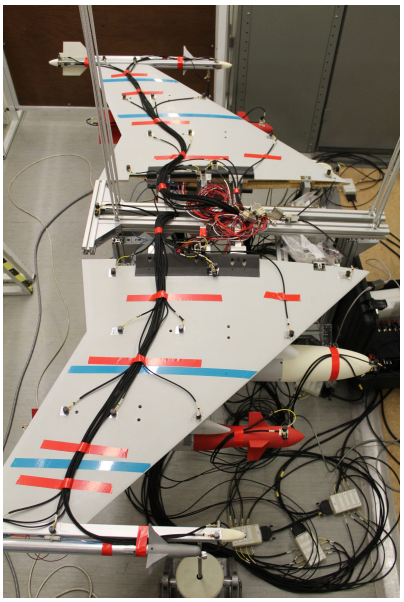

(b) Instrumentation and cabling.

Figure 5: Photos from Reference test B.

modes of interest via pre-test analysis of the finite element model. In total two input channels and 43 outputs channels were used. A LMS SCADAS Recorder with 64 channels available was used together with Siemens LMS Testlab 17 for control and data acquisition. The post-processing was done as described for reference test A.

Table 3: Results of Reference test B as compared to the nominal FE model

Experimental results			Nominal FE-model					
Mode #	Freq Hz	Gen mass kg	Mode #	Freq Hz	Gen mass kg	Freq diff %	MAC -	Description -
1	12.94	1	7	12.11	1	-6.4	0.98	ASWT
2	13.17	2	9	14.90	1	13.1	0.87	SWB
3	13.98	1	8	13.06	2	-6.6	0.95	SWT
4	21.87	6	10	23.82	3	8.9	0.96	ASWB
5	52.18	3	11	62.77	2	20.3	0.81	2nd SWB
6	55.49	2	12	65.96	1	18.9	0.89	2nd ASWB

The second and third eigenmodes, symmetric wing bending (SWB) and symmetric wing torsion (SWT), appear in different order in the finite element model compared to the experimental results, see Table 3. The torsion modes are close in frequency and shape to the experimental results, but the finite element wings appear to be too stiff in bending.

4.3 Experimental testing of each individual wing

These tests were performed once all the wings had been shipped and gathered in the same location. Each wing was suspended from a beam for an overhead crane, initially with inelastic nylon ropes attached to a metal spring in the end as in Figure 6a. Even though the wing is suspended out of the plane of vibration this gave rise to noisy measurements, as the spring was very stiff. This suspension setup was instead replaced with elastic shock-cord from a marine

supply store nearby, see Figure 6b. A double loop of shock cord gave suitably low rigid body modes, at around 1/10 of the first elastic mode.

A mobile LMS SCADAS Recorder 02 test system was used together with a very light weight Saab-built impact hammer. A total of 9 channels were used, divided between one input channel for the impact hammer and eight output channels for the accelerometers. Post-processing was done as described for reference test A.

Each wing had a wing tip pylon mounted to be sure to measure a system with clear torsion modes, since both reference tests had shown issues with correlation of the finite element torsion modes to the measured ones.

The results for wing set 2.0 can be seen in Table 4, and for wing set 2.1 in Table 5.

(a) Initial suspension setup. (b) Updated suspension setup.

Figure 6: Comparison of suspension with stiff cord and spring, and with elastic cord. Note internal pneumatic cabling has been fastened to the elastic cord.

Table 4: Results of the tap test of wing set 2.0

	Left Wing		Right Wing		
Mode #	Freq Hz	Damp ζ [%]	Freq Hz	Damp ζ [%]	Diff %
1	21.03	1.22	23.19	1.12	9.3
2	45.79	1.14	47.53	3.24	3.7
3	90.20	1.41	93.16	1.28	3.2
4	140.56	1.01	144.47	1.02	2.7
5	156.98	1.41	162.31	1.13	3.3

Table 5: Results of the tap test of wing set 2.1

	Left Wing		Right Wing		
Mode #	Freq Hz	Damp ζ [%]	Freq Hz	Damp ζ [%]	Diff %
1	21.06	2.17	21.68	1.28	2.9
2	43.07	3.44	44.54	1.87	3.3
3	89.80	1.42	91.45	1.25	1.8
4	138.63	1.18	142.17	1.07	2.5
5	157.62	1.13	161.56	1.67	2.4

5 MODEL UPDATE

A manual sensitivity analysis showed that the stiffness of the composite shells are of significant importance for the wing modes frequencies, while changing the modulus of elasticity of the foam core, the center of thickness glass-fiber structure, or the fuselage attachment has minimal impact on the eigenfrequencies. The modulus of elasticity of the unidirectional weave and weft axes, as well as the in-plane and transverse shear modulo for the material and the thickness of the layup layers are chosen as design variables. The surface of the wing is divided into 28 sections where each one can vary independently in thickness. Importantly, the angle of the unidirectional weave is of high importance for the order, and relative distance to each other, of the wing modes. The angle θ of the unidirectional weave in the composite wing shell is also chosen as a design variable.

The optimization problem described in Equation 1 with the choice of design variables above was formulated and solved using MSC Nastran SOL200. [8] MATLAB scripts were used to create most of the NASTRAN input data, such as design variables, frequency and MAC constraints, and equations for the input function.

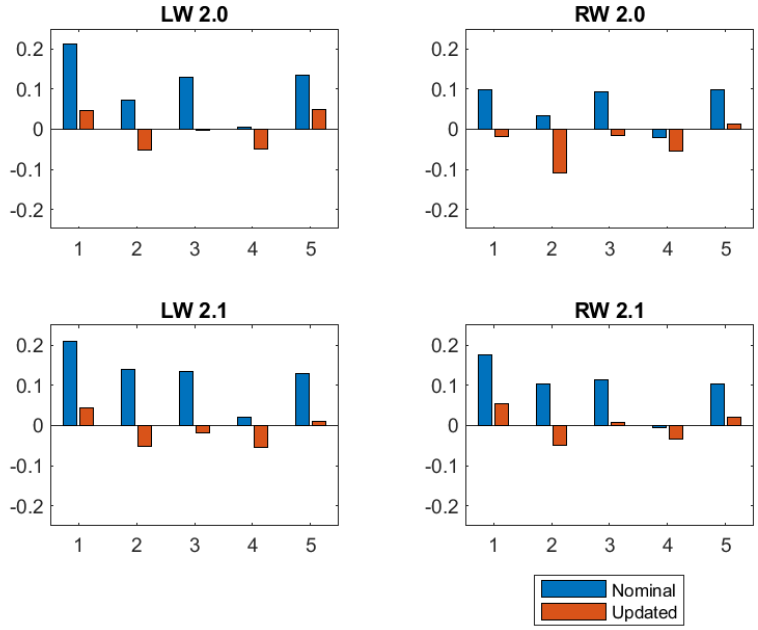

Figure 7: Relative frequency error for each wing before and after update, as compared to the tap test.

6 THE UPDATED FINITE ELEMENT MODELS

The model update process results in finite element wing models with improved correlation to the experimental results for all four test objects. Figure 7 shows the relative deviation from the experimental results for the nominal and the updated model. Figure 8 shows the mode shape correlation as described by the MAC-index, with a distinct improvement on Mode 4 (a torsional mode) for each wing. The mode shapes of the updated finite element model for the left wing of wing set 2.0 can be seen in Figure 9.

When assembling the updated models in a set that corresponds to reference test A and reference test B the result is more mixed. For reference test A, see Table 6, several bending modes have slightly worse correlation to the corresponding experimental mode shapes, but the torsional

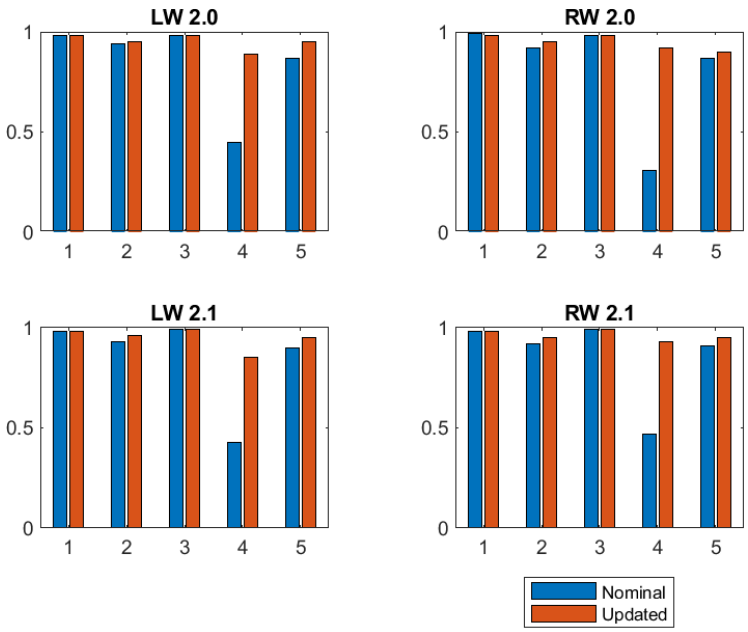

Figure 8: MAC-index for each wing before and after update, as compared to the tap test.

ones are improved in that the finite element model describes separate torsion modes for the left wing and the right wing.

The updated models for reference test B, see Table 7, results in a small frequency deviation between finite element and experimental modes, however while the frequency error is now smaller for the symmetric wing bending mode, the mode shape correlation as measured by the MAC-index has deteriorated. This is due to a phase difference between the wing tip torsion and the coupled body deflection.

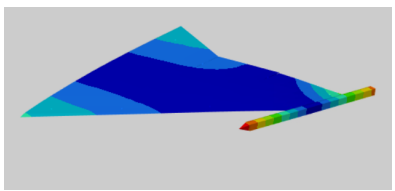

(a) Mode 7.

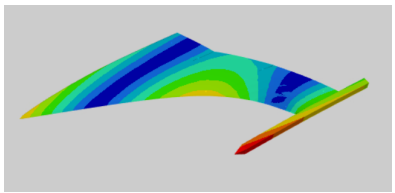

(b) Mode 8.

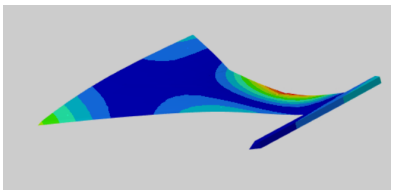

(c) Mode 9

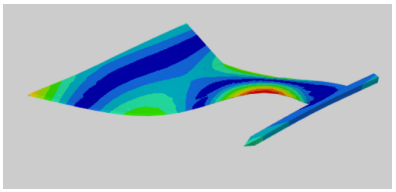

(d) Mode 10.

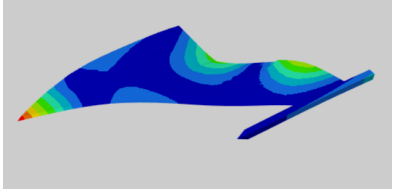

(e) Mode 12.

Figure 9: Mode shapes of the updated model for LW 2.0.

Table 6: Results of Reference test A (wing set 2.0) as compared to the updated FE model

Experimental results			Updated FE-model					
Mode #	Freq Hz	Gen mass kg	Mode #	Freq Hz	Gen mass kg	Freq diff %	MAC -	Description -
1	7.35	69	2	7.02	49	-4.5	0.80	System pitch
2	9.66	3	3	10.56	1	9.2	0.93	ASWB
3	10.09	4	4	10.96	1	8.6	0.91	SWB
4	13.76	12	5	13.80	1	0.3	0.73	ASWT
5	14.80	10	6	14.97	1	1.1	0.91	SWT
8	46.45	7	14	52.19	3	12.4	0.87	2nd ASWB
9	52.22	2	16	67.65	2	10.4	0.88	2nd SWB

Table 7: Results of Reference test B (wing set 2.1) as compared to the updated FE model

Experimental results			Updated FE-model					
Mode #	Freq Hz	Gen mass kg	Mode #	Freq Hz	Gen mass kg	Freq diff %	MAC -	Description -
1	12.94	1	7	12.50	1	-3.4	0.97	ASWT
2	13.17	2	8	13.56	1	3.6	0.44	SWB
3	13.98	1	9	13.74	2	-1.7	0.82	SWT
4	21.87	6	10	21.60	3	-1.2	0.97	ASWB
5	52.18	3	11	55.72	2	6.8	0.79	2nd SWB
6	55.49	2	12	63.38	1	14.2	0.90	2nd ASWB

7 FLUTTER CHARACTERISTICS OF THE UPDATED MODEL

The wing design process resulted in a nominal critical flutter dynamic pressure of about 150 psf according to [2]. This is in agreement with the nominal model used in this paper. The nominal model is largely the same as the initial design model, but it has been subject to a mass properties update after the weighing during reference test B. For flutter prediction, only the relevant configuration is considered. That is the full model, mounted on the TDT sting as in reference test A with wing set 2.0.

NASTRANs SOL145 with the PK-method was used for dynamic aeroelastic analysis flutter analysis of this configuration. For the the nominal model as described above this resulted in a flutter dynamic pressure of 167 psf at $M = 0.5$, as shown in Table 8.

Thereafter, four different updated configurations were put together and analysed. Each configuration used a different combination of updated left and right wings from both wing set 2.0 and wing set 2.1. The full series is shown in Table 8.

Changing the right wing between sets is shown to have minimal impact, while switching the left wing from the nominal, to one correlating with wing set 2.0 and to one correlating to wing set 2.1 has a significant impact on flutter dynamic pressure. A root locus plot for the critical flutter points for configurations UPD1 and UPD3 is shown in Figure 10.

Table 8: Critical flutter dynamic pressure in NASTRAN, at $M = 0.5$.

Configuration #	Description	Critical mode #	Critical dynamic pressure psf
NOM	LW 2.0 / RW 2.0	7	159.04
UPD1	LW 2.0 / RW 2.0	5	125.38
UPD2	LW 2.0 / RW 2.1	5	125.38
UPD3	LW 2.1 / RW 2.0	5	160.47
UPD4	LW 2.1 / RW 2.1	5	160.47

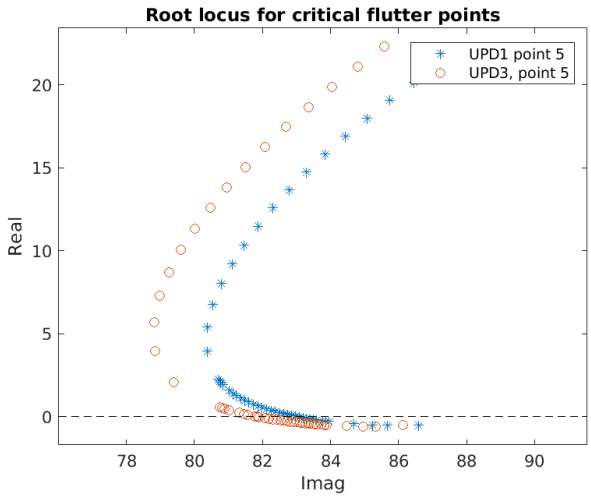

Figure 10: Root locus plot of the critical modes for UPD1 and UPD3.

8 CONCLUSIONS

A relatively large spread in flutter dynamic pressure is obtained using a nominal and updated finite element model respectively. This is an indication of how important a correct structural model is, and that experimental work is essential to ensure robustness of analytical models.

Modal testing has shown that the manufactured wing differs from the theoretical wing design, and importantly that the individual wings differ from each other. The model updating process has resulted in finite element models better matching the experimental results. There are still differences between the finite element models predictions and the experimental results. Some of these differences can be attributed to the other structural properties of the model, such as the fuselage, fin and canards. Other differences is a result of the model update process. By testing the wing with wing tip pylons mounted the torsion modes have been well captured, but the wing bending modes less so. Using multiple configurations, i.e. a free-free wing without the wing tip pylon as well, as an input for the model update process would probably result in a more well rounded finite element model. The reference tests could possibly be used, but would diminish in value as references.

9 REFERENCES

[1] Ringertz, U., Eller, D., Keller, D. F., et al. (2017). Design and testing of a full span aeroelastic wind tunnel model. In *19th International Forum on Aeroelasticity and Structural Dynamics*, vol. 3. pp. 1880–1899.

[2] Ringertz, U. (2019). Wing design for wind tunnel flutter testing. In *20th International Forum on Aeroelasticity and Structural Dynamics*, vol. 3. pp. 2102–2112.

[3] Stanford, B. K. and Massey, S. J. (2017). Uncertainty quantification of the fun3d-predicted nasa crm flutter boundary. In *SciTech Forum*, NF1676L-24499.

[4] TE Connectivity Sensor (2018). *OPTIMUS VERSION-2 PRESSURE SCANNING SYSTEM*. TE Connectivity.

[5] Cauberghe, B. (2004). *Applied frequency-domain system identification in the field of experimental and operational modal analysis*. Ph.D. thesis, Vrije Universiteit Brussel.

[6] Allemang, R. J. (2003). The modal assurance criterion–twenty years of use and abuse. *Sound and vibration*, 37(8), 14–23.

[7] Holmberg, E. (2019). Fe-model update after gvt of a gripen e test aircraft. In *20th International Forum on Aeroelasticity and Structural Dynamics*.

[8] MSC Nastran 2018 (2021). *Design Sensitivity and Optimization User's Guide*. MSC Software Corporation.

COPYRIGHT STATEMENT